# Characterization of N-doped multilayer graphene grown on 4H-SiC (0001)

Hakim Arezki, Kuan-I Ho, Alexandre Jaffré, David Alamarguy, J Alvarez, Jean-Paul Kleider, Chao-Sung Lai, Mohamed Boutchich

# Characterization of N-doped multilayer graphene grown on 4H-SiC (0001)

Hakim Arezkihakim.arezki@lgep.supelec.frKuan-I HoAlexandre Jaffré, David Alamarguy, José Alvarez, and Jean-Paul KleiderChao-Sung LaiMohamed Boutchich

Citation: **1649**, 8 (2015); doi: 10.1063/1.4913537
View online: http://dx.doi.org/10.1063/1.4913537
View Table of Contents: http://aip.scitation.org/toc/apc/1649/1
Published by the American Institute of Physics

# Characterization of N-doped multilayer graphene grown on 4H-SiC (0001)

Hakim Arezki[1, a], Kuan-I Ho[2], Alexandre Jaffré[1], David Alamarguy[1], José Alvarez[1], Jean-Paul Kleider[1], Chao-Sung Lai[2], Mohamed Boutchich[1]

[1]*LGEP, CNRS UMR8507, SUPELEC, Univ Paris-Sud, Sorbonne Universités - UPMC, Univ Paris 06, 11 rue Joliot-Curie, Plateau de Moulon, 91192 Gif-sur-Yvette Cedex, France*
[2] *Department of Electronic Engineering, Chang Gung University, No. 259, Wen-Hua 1st Rd, Kweishan, Taoyuan 333, Taiwan, R.O.C*

a) Corresponding author: hakim.arezki@lgep.supelec.fr

**Abstract.** Large-area graphene film doped with hetero-atoms is of great interest for a wide spectrum of nanoelectronics applications, such as field effect devices, super capacitors, fuel cells among many others. Here, we report the structural and electronic properties of nitrogen doped multilayer graphene on 4H-SiC (0001). The incorporation of nitrogen during the growth causes an increase in the D band on the Raman signature indicating that the nitrogen is creating defects. The analysis of micro-Raman mapping of G, D, 2D bands shows a predominantly trilayer graphene with a D band inherent to doping and inhomogeneous dopant distribution at the step edges. Ultraviolet photoelectron spectroscopy (UPS) indicates an n type work function (WF) of 4.1 eV. In addition, a top gate FET device was fabricated showing n-type I-V characteristic after the desorption of oxygen with high electron and holes mobilities.

## INTRODUCTION

Since its discovery, graphene has attracted tremendous interest for condensed physics and material science [1,2,3,4]. To date, researchers keep on optimizing synthesis technologies i.e. mechanical exfoliation, oxidation of graphite, thermal decomposition of SiC[5], liquid-phase exfoliation of graphite, chemical vapour deposition (CVD) [6]. CVD and SiC graphene exhibit opto-electronic properties that could potentially outperform any alternative material and permit its implementation into a wide spectrum of applications with devices like field effect transistors (FETs) [7], solar cells, sensors. In particular triltroayer graphene attracts a lot of interest [8,9,10]. The electronic bands structure of both stable forms of trilayer graphene – i.e., Bernal (ABA) and rhombohedral (ABC) [5], differ for the crystallographic stacking of the individual carbon layers.Nevertheless to consider applications the electronic properties of synthesized graphene still remain to be tailored to become competitive. For that purpose, a substantial part of the research effort is devoted to develop doping strategies using III-V elements i.e. boron (B) and nitrogen (N) for p and n type respectively [11,12,13]. However considering the structure of graphene, doping must be adapted to its technology. Among the favoured approaches are the modulation of the electronic properties through *in situ* doping during synthesis [14,15] and charge transfer using hetero-interfaces e.g. nano colloids, polymers, self-assembly monolayers[16,17]. Regarding in situ doping strategy, one method consists of introducing nitrogen during the growth process. A second approach consists of annealing the sample post growth under nitrogen atmosphere [15]. Here, we report on the preparation of large area N-doped multilayer graphene on 4H-SiC (0001). The N-doped graphene was formed on SiC substrate at high temperature. Nitrogen species were incorporated spontaneously into the graphene during the cooling of the sample at room temperature and under nitrogen flux. The N doped graphene were characterized by Raman micro mapping spectroscopy and UPS spectroscopy.

*The Irago Conference 2014*
AIP Conf. Proc. 1649, 8-13 (2015); doi: 10.1063/1.4913537

## SAMPLE PREPARATION

The different samples of graphene studied in this work were produced via a two-step process starting with a substrate of 4H-SiC (0001). Prior to graphitization, the substrate was hydrogen etched (100% $H_2$) at 1550 °C to produce well-ordered atomic terraces of SiC. Subsequently, the SiC sample was heated to 1000 °C and then further heated to 1525 °C in an Ar atmosphere. Samples were then cooled down for 5 min from 1525°C to room temperature under a nitrogen flow of 500 sccm at 800 mbar. These samples are labelled as N-doped graphene. The layers were then transferred *ex-situ* from the growth chamber to Raman spectroscopy and UPS measurement systems.

The Raman measurements were performed with a frequency-doubled NdYag laser operating at 532 nm as excitation source with up to 20 mW continuous wave output power. The spectra were recorded through a 300 mm imaging spectrometer equipped with both a 600 lines/mm and 1800 lines/mm grating, and a back-illuminated CCD. A 100x dry and oil immersion objective with respectively a numerical aperture (NA) of 0.9 and 1.4, and a 50 µm core diameter multimode fiber acting as a pinhole were used to collect the Raman signal. The expected lateral spatial resolution in the x-y plane can reach 150 nm (NA=1.4) and 250 nm (NA=0.9). A particular attention was paid to the incident laser power density to avoid local heating effects that can induce a shift of the Raman peaks. The mapping was collected using a piezoelectric stage with a spatial resolution of 250 nm.

.

## Morphology

The nucleation and the growth mechanisms of graphene strongly rely on the SiC morphology studied by atomic force microscopy (AFM). The AFM image was acquired on the same area scanned by micro Raman mapping. Figure 1 displays the surface morphology measured by AFM. The AFM image shows topography with a high step density of 10-15nm height and atomically flat terraces of 700 nm wide on average. We observe a good surface coverage and very little step bunching across the scanned area owing growth temperature of 1525°C under argon atmosphere. On the defect-free region of the sample, the terraces may extend undisturbed over 40µm as can be seen on the image.

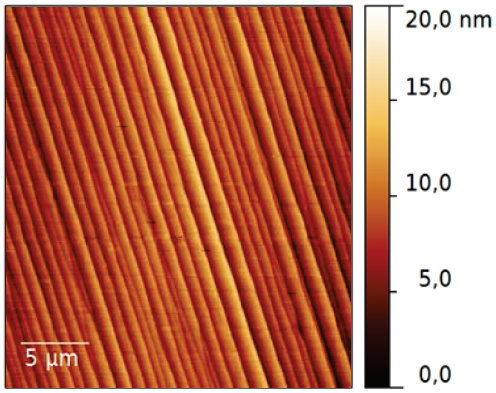


**FIGURE 1.** AFM topography of epitaxial graphene sample.

## RESULTS AND DISCUSSION

We performed UPS analysis to determine the shift in work function induced by N atoms and verify the nature of the doping of graphene layers. UPS data were acquired several times from the overall sample and the averaged results are shown in Figure 2. This shows the UPS spectra around the secondary electrons cut-off region of the pristine and N-doped graphene. The position of the Fermi level was calibrated using a gold sample. The secondary electron cut-off was determined by extrapolating two solid lines from the background and straight onset in the secondary electron cut-off region of the spectra. WF is determined from the secondary electron cut-off as $WF = h\nu - E_{th}$, where $h\nu$ and $E_{th}$ are the photon energy of excitation light (He I discharge lamp, 21.2 eV) and the secondary electron cut-off

energy, respectively. As a reference, we utilized a sample of pristine monolayer graphene but without N-doping, the WF measured is 4.3 eV, similar values have been reported previously. As a result, we can conclude that the N-doping process implemented in this work has demonstrated its effectiveness to shift to a minimum of 0.2 eV the WF from 4.3 eV to 4.1 eV confirming the n-type nature of the material, figure 2.

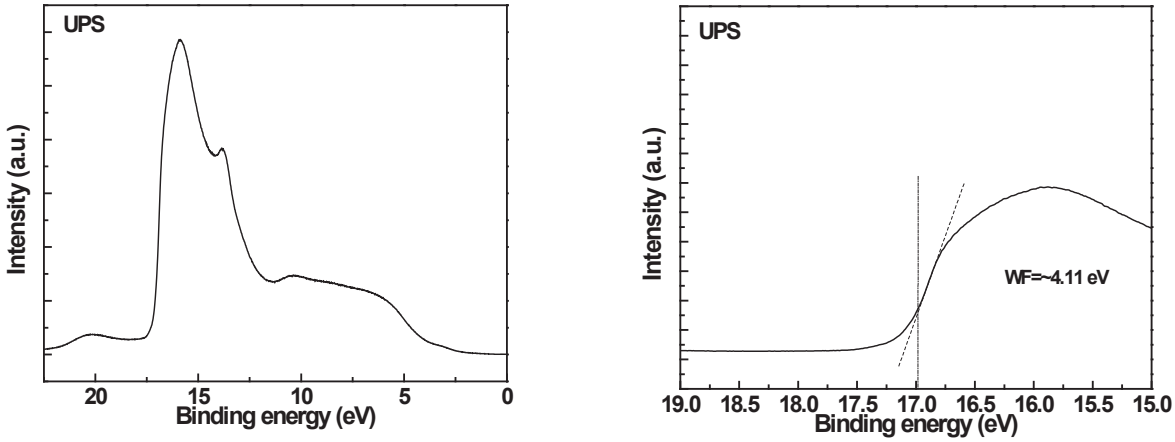


**FIGURE 2.** UPS spectra of the N-doped graphene. Left panel shows global spectrum and right panel shows the secondary electron cut-off and the Fermi level regions respectively to determine the work function (WF).

To investigate the electronic properties of the N-doped graphene, we have carried out coupled Raman micro-mapping to AFM to record maps across a sample area of 20x20µm². Note that single spectrum acquired at one location would not reflect the defect distribution across the sample as well as the N doping. The data reduction of the overall spectra acquired on this area allows us to extract the most representative bands i.e. D, G, 2D shifts as well as the $I_D/I_G$ ratios to provide information on disorder and defect distribution. Figure 3 displays the Raman signatures of an N-doped samples showing incomplete growth in zone 1, figure 3.

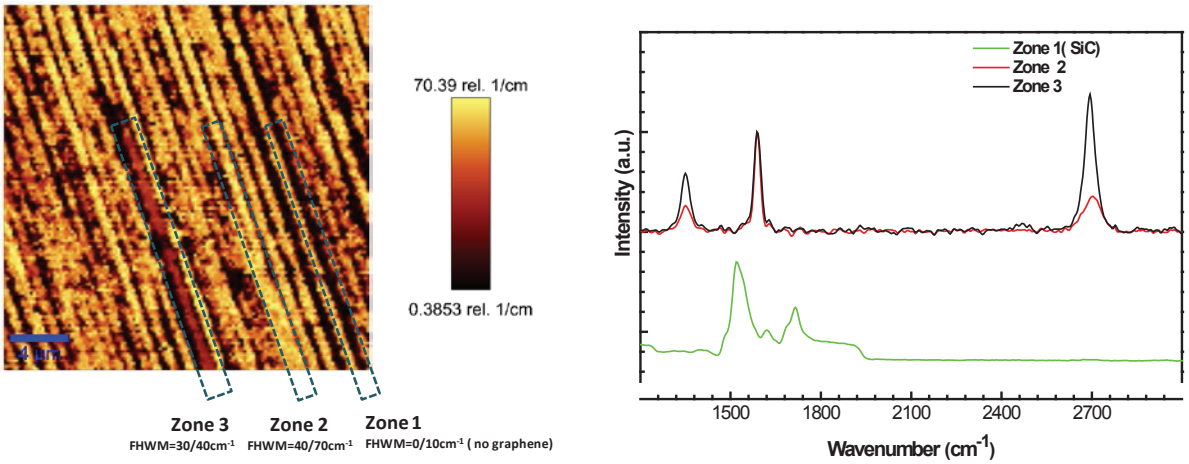


**FIGURE 3.** left) 2D band full width half maximum mapping showing 3 different zones. Multilayer (zone 2 and 3) whereas zone 1 shows the contribution of the SiC substrate when graphene is missing. Right) spectra for the various zones showing, D, G and 2D bands.

The epitaxial graphene grown here exhibits a G peak induced by the zone- center $E_{2g}$ phonon close to 1570 $cm^{-1}$ and a 2D peak corresponding to the overtone of the zone-boundary $A_{1g}$ phonon at 2700 $cm^{-1}$ [18,19]. All traces show the main features of graphene as well as SiC in the 1100-3000 $cm^{-1}$ region. N-doped traces exhibit a D peak close to 1360 $cm^{-1}$ increasing with $I_D/I_G$ demonstrating the inhomogeneous defect distribution across the sample [20]. In

addition, we observe a weak D' peak at 1620 $cm^{-1}$ which is a signature of disorder on the N-doped sample also induced by defects. We note that the G and 2D peaks intensity and FWHM vary across the sample. This indicates the thickness inhomogenity as well as the disorder caused by the nitrogen incorporation.

Figure 4(a,b,c,d) displays the G, 2D band as well as the FWHM of the 2D band mappings and the $I_D/I_G$ ratio mapping. . Figure 4(a,b) shows the G and 2D shifts mappings acquired over the same area as the AFM image, figure 3(a). for both bands, we observe shifts across the sample that can be related to the doping as well as the biaxial strain [21]. At this stage considering the complex growth mechanism of N-doped graphene on 4H-SiC (0001), it is difficult to conclude on charge transfer just analyzing the Raman signatures. Indeed, the interface layer intrinsic to the growth on SiC substrate has a strong contribution to the Raman signature between 1200-1600 $cm^{-1}$ and the subsequent analysis is particularly complex. Nevertheless, the doping nature has already been revealed by the aforementioned UPS measurements. Still the presence of both G and 2D bands across the overall area indicates that graphene has been grown everywhere in this sample. Figure 4(c) displays the FWHM of the 2D band. The FWHM varies from 24 $cm^{-1}$ up to 100$cm^{-1}$ clearly indicating the presence of monolayer graphene and a predominent trilayer graphene with FWHM ~80 $cm^{-1}$. Figure 4(d) displays the variation across the sample of the $I_D/I_G$ ratio. This ratio indicates the inhomogeneous doping and defect distribution. Here we observe that the $I_D/I_G$ ratio ranges from very low value to as high as 1.744. Dark areas reflect low $I_D/I_G$ ratio on the map indicating a smaller defect density. Although, the pattern follows regular stripes, the defect density and therefore the dopant distribution is clearly non uniform.

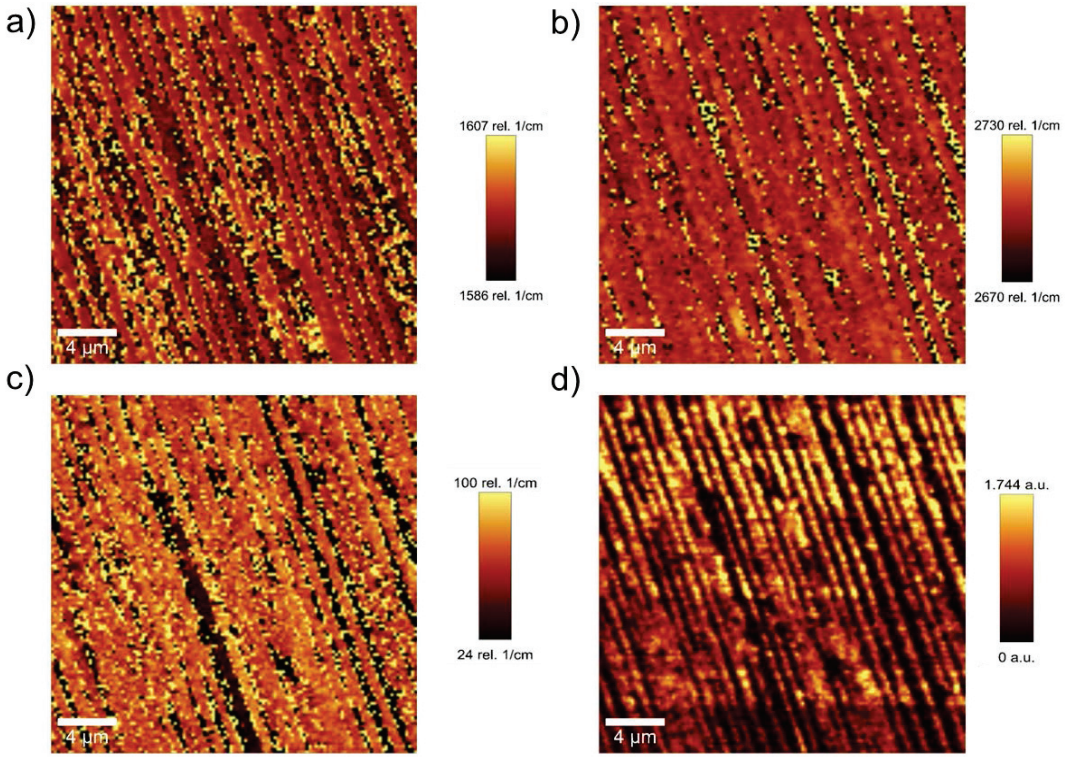


I

**FIGURE 4.** a) G band Raman shift mapping over the area scanned with AFM. The SiC contribution affects the picture but graphene is present all over the area, b) 2D band Raman Shift mapping showing homogenous picture as opposed to the G band, c) 2D band FWHM mapping indicating the presence of mono to multilayer graphene. (d) $I_D/I_G$ mapping taken on the same area scanned by AFM.

At last a top gate FET device was fabricated by optical lithography and 7nm thick aluminum oxide ($Al_2O_3$) gate oxide. Al top gate was deposited by e-beam evaporation. The device was tested at room temperature. Figure 5 shows I-V characteristics indicating ambipolar transistor effect. We first acquired the I-V before pumping down (red trace). As oxygen has been adsorbed on the graphene surface, the $V_D$ is located at ~3V typically p-type and the electron hole mobilities seem low as indicted by the small I-V slopes. However once the device is pumped down to $10^{-5}$ mbar

the $V_D$ shifts down to -1V and the device clearly reveals the n-type doping character of N incorporation of the graphene [22]. Graphene exposed to air tends to be p-type doped due to its interaction with the $H_2O/O_2$ so pumping break those bonding and brings graphene back to its intrinsic $V_{Dirac}$ [24]. This top gate FET exhibits interesting room temperature mobilities of 1350 cm²/Vs and 850 cm²/Vs for hole and electron respectively.

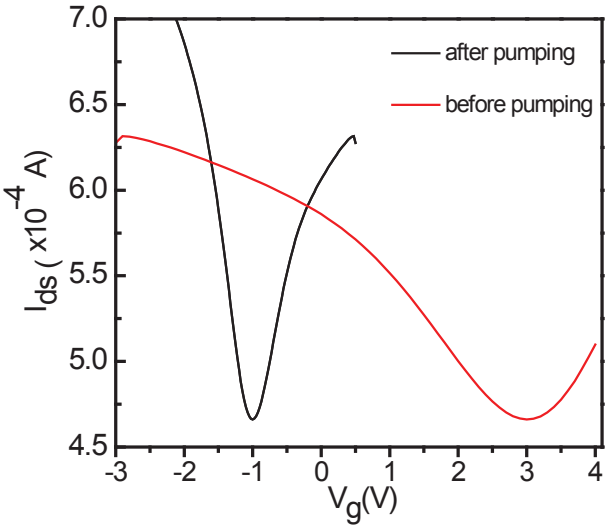


**FIGURE 5.** I-V characteristics of top gate graphene FET. The red curve shows the I-V before pumping whereas the black curve shows the I-V after oxygen desorption revealing the n-type nature of the graphene with a VD located at -1V.

## CONCLUSION

In summary, we have investigated a non-destructive doping approach to insert nitrogen into predominantly trilayer graphene on SiC substrate. The nitrogen incorporation into the graphene network reduces the work function from 4.4 eV for the pristine graphene to 4.1 eV for the N-doped graphene as observed by UPS. The Raman mappings show a correlation between graphene areas and defect distribution which appear to be inhomogeneous from the $I_D/I_G$ ratio. A top gate FET device was fabricated showing n-type I-V characteristic after the desorption of oxygen.

## ACKNOWLEDGMENTS

Authors wish to thank Dr A.Ouerghi from Laboratoire de Photonique et de Nanostructures for providing the samples As well as the Labex NanoSaclay under grant 120098, the French Ministère des affaires étrangères et européennes (MAEE) and the Centre National de la Recherche Scientifique (CNRS) for their financial support in the STIC ASIA program.

## REFERENCES

1. K.S. Novoselov, A.K. Geim, S.V. Morozov, D. Jiang, M.I. Katsnelson, I.V. Grigorieva, S.V. Dubonos, and A.A. Firsov, Nature **438**, 197 (2005).
2. Z. Jiang, Y. Zhang, Y.-W. Tan, H.L. Stormer, and P. Kim, Solid State Commun. **143**, 14 (2007).
3. E. Pallecchi, F. Lafont, V. Cavaliere, F. Schopfer, D. Mailly, W. Poirier, and A. Ouerghi, Sci. Rep. **4**, 4558 (2014).
4. E. Pallecchi, M. Ridene, D. Kazazis, C. Mathieu, F. Schopfer, W. Poirier, D. Mailly, and A. Ouerghi, Appl. Phys. Lett. **100**, 253109 (2012).
5. B. Lalmi, J.C. Girard, E. Pallecchi, M. Silly, C. David, S. Latil, F. Sirotti, and A. Ouerghi, Sci. Rep. **4**, 4066 (2014).
6. S. Bae, H. Kim, Y. Lee, X. Xu, J.-S. Park, Y. Zheng, J. Balakrishnan, T. Lei, H. Ri Kim, Y.I. Song, Y.-J. Kim, K.S. Kim, B. Özyilmaz, J.-H. Ahn, B.H. Hong, and S. Iijima, Nat. Nanotechnol. **5**, 574 (2010).

7. L. Britnell, R.V. Gorbachev, R. Jalil, B.D. Belle, F. Schedin, A. Mishchenko, T. Georgiou, M.I. Katsnelson, L. Eaves, S.V. Morozov, N.M.R. Peres, J. Leist, A.K. Geim, K.S. Novoselov, and L.A. Ponomarenko, Science **335**, 947 (2012).
8. T. Cui, R. Lv, Z.-H. Huang, H. Zhu, Y. Jia, S. Chen, K. Wang, D. Wu, and F. Kang, Nanoscale Res. Lett. **7**, 1 (2012).
9. A. Singh, M.A. Uddin, T. Sudarshan, and G. Koley, Small **10**, 1555 (2014).
10. X. An, F. Liu, and S. Kar, Carbon **57**, 329 (2013).
11. E. Vélez-Fort, E. Pallecchi, M.G. Silly, M. Bahri, G. Patriarche, A. Shukla, F. Sirotti, and A. Ouerghi, Nano Res. **7**, 835 (2014).
12. B. Guo, Q. Liu, E. Chen, H. Zhu, L. Fang, and J.R. Gong, Nano Lett. **10**, 4975 (2010).
13. L.S. Panchakarla, K.S. Subrahmanyam, S.K. Saha, A. Govindaraj, H.R. Krishnamurthy, U.V. Waghmare, and C.N.R. Rao, Adv. Mater. **21**, 4726 (2009).
14. D. Wei, Y. Liu, Y. Wang, H. Zhang, L. Huang, and G. Yu, Nano Lett. **9**, 1752 (2009).
15. Emilio Velez-Fort, Claire Mathieu, Emiliano Pallecchi, Marine Pigneur, Mathieu G Silly, Rachid Belkhou, Massimiliano Marangolo, Abhay Shukla, Fausto Sirotti, Abdelkarim Ouerghi, ACS Nano, **6**, 10893 (2012).
16. S.M. Kim, K.K. Kim, Y.W. Jo, M.H. Park, S.J. Chae, D.L. Duong, C.W. Yang, J. Kong, and Y.H. Lee, ACS Nano **5**, 1236 (2011).
17. S. Das, P. Sudhagar, E. Ito, D. Lee, S. Nagarajan, S.Y. Lee, Y.S. Kang, and W. Choi, J. Mater. Chem. **22**, 20490 (2012).
18. C. Casiraghi, A. Hartschuh, E. Lidorikis, H. Qian, H. Harutyunyan, T. Gokus, K.S. Novoselov, and A.C. Ferrari, Nano Lett. **7**, 2711 (2007).
19. L. Zhao, R. He, K.T. Rim, T. Schiros, K.S. Kim, H. Zhou, C. Gutierrez, S.P. Chockalingam, C.J. Arguello, L. Palova, D. Nordlund, M.S. Hybertsen, D.R. Reichman, T.F. Heinz, P. Kim, A. Pinczuk, G.W. Flynn, and A.N. Pasupathy, Science **333**, 999 (2011).
20. H. Wang, T. Maiyalagan, and X. Wang, ACS Catal. **2**, 781 (2012).
21. Rank O, Tsoukleri G, Parthenios J et al, 3rd Int. Conf. NANOCON Brno Czech Repub. Nanocon (2011).
22. A. Das, S. Pisana, B. Chakraborty, S. Piscanec, S.K. Saha, U.V. Waghmare, K.S. Novoselov, H.R. Krishnamurthy, A.K. Geim, A.C. Ferrari, and A.K. Sood, Nat. Nanotechnol. **3**, 210 (2008).
23. K. NOVOSELOV, H. KRISHNAMURTHY, A. GEIM, A. FERRARI, and A. SOOD, (2008).
24. D.-W. Shin, H.M. Lee, S.M. Yu, K.-S. Lim, J.H. Jung, M.-K. Kim, S.-W. Kim, J.-H. Han, R.S. Ruoff, and J.-B. Yoo, ACS Nano **6**, 7781 (2012).